

Towards an in silico integrated approach for testing and assessment of nanomaterials: from predicted indoor air concentrations to lung dose and biodistribution

Tsiros, P.; Cheimarios, N.; Tsoumanis, A.; Jensen, A. C. Ø.; Melagraki, G.; Lynch, I.; Sarimveis, H.; Afantitis, A.

DOI:
[10.1039/D1EN00956G](https://doi.org/10.1039/D1EN00956G)

License:
Creative Commons: Attribution (CC BY)

Document Version
Publisher's PDF, also known as Version of record

Citation for published version (Harvard):
Tsiros, P, Cheimarios, N, Tsoumanis, A, Jensen, ACØ, Melagraki, G, Lynch, I, Sarimveis, H & Afantitis, A 2022, 'Towards an in silico integrated approach for testing and assessment of nanomaterials: from predicted indoor air concentrations to lung dose and biodistribution', *Environmental Science: Nano*, vol. 9, no. 4, pp. 1282-1297. <https://doi.org/10.1039/D1EN00956G>

[Link to publication on Research at Birmingham portal](#)

General rights

Unless a licence is specified above, all rights (including copyright and moral rights) in this document are retained by the authors and/or the copyright holders. The express permission of the copyright holder must be obtained for any use of this material other than for purposes permitted by law.

- Users may freely distribute the URL that is used to identify this publication.
- Users may download and/or print one copy of the publication from the University of Birmingham research portal for the purpose of private study or non-commercial research.
- User may use extracts from the document in line with the concept of 'fair dealing' under the Copyright, Designs and Patents Act 1988 (?)
- Users may not further distribute the material nor use it for the purposes of commercial gain.

Where a licence is displayed above, please note the terms and conditions of the licence govern your use of this document.

When citing, please reference the published version.

Take down policy

While the University of Birmingham exercises care and attention in making items available there are rare occasions when an item has been uploaded in error or has been deemed to be commercially or otherwise sensitive.

If you believe that this is the case for this document, please contact UBIRA@lists.bham.ac.uk providing details and we will remove access to the work immediately and investigate.



Cite this: DOI: 10.1039/d1en00956g

Towards an *in silico* integrated approach for testing and assessment of nanomaterials: from predicted indoor air concentrations to lung dose and biodistribution†

P. Tsiros, ^a N. Cheimarios, ^b A. Tsoumanis, ^b A. C. Ø. Jensen, ^c G. Melagraki, ^d I. Lynch, ^e H. Sarimveis ^{*a} and A. Afantitis ^{*b}

Integrated approaches to testing and assessment (IATA) provide a framework for combining information from different sources (experimental, *in silico*) for hazard characterisation of chemicals, including nanomaterials (NM), based on a weight of evidence approach. Experimentally acquiring the exposure, hazard and characterisation data for NMs necessary to perform risk assessment is time-consuming and costly, thus driving demand for *in silico* models to facilitate read-across from data rich NMs to data poor ones, or to predict exposure or hazard. In this work, we present three integrated computational approaches which can be used to generate data relevant to human health risk assessment, namely the multi-box aerosol model for prediction of indoor air concentrations of NMs, the lung exposure model to determine the lung burden of NMs following acute exposures and a physiologically based pharmacokinetic (PBPK) model to determine the biodistribution of the NMs to other organs over longer timescales following inhalation. The lung exposure application is based on empirical deposition equations for calculating the deposited mass in the human respiratory system. The PBPK model extends the lung exposure model by introducing clearance terms and translocation of the NMs to the systemic circulation after passage through the air-blood barrier in the alveoli. Several exposure scenarios with varying conditions are introduced in order to compare the models in relation to the accumulated mass of NMs in the alveolar, tracheobronchial and head airways regions of the respiratory system, thus exploring their capabilities and weaknesses, and potential contribution to a NM-specific IATA for occupational exposure.

Received 19th October 2021,
Accepted 30th January 2022

DOI: 10.1039/d1en00956g

rsc.li/es-nano

Environmental significance

Nanomaterials (NMs) have become part of our daily life yet their long term and cumulative impact on human health is unknown. Experiments to understand their biodistribution and clearance are costly and ethically challenging, such that existing data are limited to specific NMs and rodent models. Computational tools are a promising way to assess the impacts of NMs exposure on humans. Despite their promise, such computational tools are currently lacking, and those that are available are not aligned in terms of inputs and outputs to facilitate risk assessment. Here, an integrated computational framework for assessing the internal deposition and distribution of NMs following exposure in an occupational setting is proposed. The computational methodology for calculation of the spatiotemporal emission profile can be further extended to include, in addition to indoor exposure, NM emissions to the surrounding environment. The tool integration connecting an external exposure model with internal exposure models for acute and chronic timescales enables users to conduct a complete *in silico* environmental risk assessment.

1. Introduction

From sunscreen and cosmetics to clothes and printer toner, nanomaterials (NMs) have become part of our daily lives. As with many natural (*e.g.*, viruses) and anthropogenic particles, NMs enter the human body through the respiratory system, and can, upon passing through the air-lung barrier, have access to the circulatory system and the whole body. However, as yet, risk assessment of the impacts of NMs on human health is still an open issue and is dependent on

^a School of Chemical Engineering, National Technical University of Athens, Athens, Greece. E-mail: hsarimv@central.ntua.gr

^b NovaMechanics Ltd, Nicosia, Cyprus. E-mail: afantitis@novamechanics.com

^c The National Research Centre for the Working Environment, Denmark

^d Hellenic Army Academy, Athens, Greece

^e School of Geography, Earth and Environmental Sciences, University of Birmingham, Birmingham, UK

† Electronic supplementary information (ESI) available. See DOI: 10.1039/d1en00956g

‡ These authors contributed equally.



costly and time-consuming experiments on animals in many cases. Risk assessment related to NMs requires information on both the likelihood of exposure to the NMs, in terms of concentration, duration and form, and the hazard posed to the organisms the NMs come into contact with. Case-by-case determination of exposure and hazard data for each application and individual NM variant is not possible due to the time and cost required, as well as the ethical challenges inherent in animal experimentation, and thus there is a strong motivation to develop *in silico* models that can predict human exposure to, and impacts of, NMs based on a reduced set of input parameters, as part of an integrated approach to testing and assessment (IATA). An example of the use of computational tools in the context of risk assessment was introduced by Mollá *et al.*,¹ who recently proposed NanoSerpa, an application for the risk assessment of NMs in the insurance sector, which was developed by integrating hazard-related data and optimized exposure models. The focus of NanoSerpa is on estimation of the insurance liability arising from accidental NMs spills during production, transport or use of NMs-containing products, based on input data regarding the type of NM and the accident scenario, utilising probabilistic models to predict emission, health hazard values and risk indices.¹ Other tools for risk assessment of NMs are also emerging, including hazard classification tools,^{2–4} screening level models for predicting NMs transport and concentrations in the environment such as SimpleBox4Nano,^{5,6} and probabilistic models of NMs flows^{7,8} from production to waste treatment. However, the various models have yet to be made inter-operable and combined into an overall IATA in order to facilitate complete (*in silico*) risk assessment.

Such integrated *in silico* models are potentially of enormous value in the context of NMs risk assessment and more broadly for life cycle impact assessment (LCIA), an important approach for analysing, evaluating, understanding and managing the environmental and health effects of NMs based on inventories of inputs and outputs.⁹ Both risk assessment (RA) and LCIA have two components, one referring to and characterising the exposure to a toxicant and one characterising the health effects that accompany the exposure. In particular, external exposure models can calculate the spatiotemporal evolution of the concentration of NMs emitted from one or multiple sources, while biokinetics models can transform the external concentration into organ burdens. The internal mass can then be compared with hazard thresholds to evaluate the risk associated with possible adverse health effects. An example of a complete LCIA workflow was presented by Tsang *et al.*,¹⁰ who proposed a dynamic model that involved integration of multiple *in silico* tools for quantifying the emissions and effects of NMs to human health in an occupational setting. The tools presented in our work aim at generating exposure data relevant to RA and LCIA and the extensive comparison of the lung models performed herein uncovers the relative strengths and weaknesses of the different modelling approaches in

terms of their data input needs and the robustness and utility of their outputs.

In this work we present two integrated approaches for assessment of the accumulated doses of NMs in the human respiratory system following exposure to NMs in indoor environments, which can be used in risk assessment and LCIA studies. The approach consists of two parts; the first part is to evaluate the airborne concentration of the specific NM in the indoor environment and the second part is to compute the accumulated mass in the respiratory system. The concentration of the NMs in the indoor environment is calculated with a multi-box aerosol model. The multi-box aerosol model is based on an aerosol dynamics particle population balance equation.¹¹ Although several models have been proposed for the calculation of the concentration of the NMs based on Eulerian,¹² Gaussian plume,^{13,14} Lagrangian,^{15,16} and Markov chain models,¹⁷ the multi-box aerosol model is the most well-established.¹⁸ The multi-box aerosol model is based on the assumption of a well-mixed chamber where the NM concentrations are instantly mixed in the entire volume.¹¹ However other models have also been proposed of imperfectly mixed chambers¹⁹ or which consider the existence of walls that restrict the flow^{20–23} or include ventilation and recirculation.^{24–26}

The second part of the model is the calculation of the accumulated NM mass in the human respiratory system. In the present work, two models are used and compared, the lung exposure model and an advanced physiologically-based pharmacokinetic (PBPK) modelling approach. The lung exposure model is based on empirical equations built upon the International Commission on Radiological Protection (ICRP) model for the respiratory system²⁷ while the PBPK model is built using rat inhalation data which was extrapolated to humans by adjusting a number of physiological and substance specific parameters and use of allometric scaling. Both models take as their input the concentration of NMs over time as calculated *via* the multi-box aerosol model. The lung exposure model supports various NMs such as black toner, TiO₂ and TiO₂ embedded with AgX, where X = O, Cl or pure Ag (so the particles are TiO₂-Ag, TiO₂-Ag₂O and TiO₂-AgCl), as well as user-defined particle size distributions, thus covering a broad range of NMs. The PBPK model currently supports only TiO₂ NMs for which biodistribution data was available, although similar models can be constructed in the future provided that biodistribution data for other NMs become available. The lung exposure model calculates the accumulated NM mass in the alveolar, tracheobronchial (TB) and head airways regions, while the PBPK model calculates the accumulated mass in many regions of the human body, including heart, spleen, brain, kidneys, liver, lower respiratory, blood, lungs interstitium and capillaries, soft tissues and skin. Compared to the Lung exposure model, the PBPK modelling approach takes into account clearance processes, *i.e.*, the removal of the NMs from the human body, which makes it more realistic especially over longer-term exposures or for



evaluation of cumulative exposures. Freely available web applications have been developed for both models, and for the multi-box exposure model, which in turn constitute part of an integrated computational framework to estimate the deposited doses of NMs in the human respiratory system after occupational/indoor inhalation as part of an overall risk assessment and/or NMs life cycle assessment framework.

The computational framework consists of three independent applications as shown in Fig. 1: a multi-box aerosol model based application, the lung exposure dose calculator and a PBPK model. The overall computation starts by selecting the NMs size-resolved emission rate in the multi-box aerosol model, which estimates the NM concentration inside the different boxes (areas) that the indoor environment has been partitioned into. The computed airborne NMs concentration in the different areas are then introduced into the lung exposure dose calculator which, based on the exposure time and the respired volume rate, estimates the deposited dose in the human respiratory system. For a more detailed output regarding the whole-body biodistribution and long-term kinetics, which takes into account clearance rates, the computed NMs concentrations from the multi-box aerosol model can also be provided to the PBPK model, which estimates the internal doses of the NMs in various tissues as a function of time. In the following sections each model is presented in detail, and the outputs are compared in terms of the utility for human risk assessment and LCIA applications as part of an *in silico* IATA.

2. Materials and methods

2.1 The multi-box aerosol model

The multi-box aerosol model,^{11,28} is based on the aerosol dynamics particle population balance equation:

$$\frac{dN_{k,i}}{dt} = J_{\text{source},k,i} + J_{\text{exchange},k,i} + J_{\text{coagulation},k,i} + J_{\text{deposition},k,i} \quad (1)$$

where $\frac{dN_{k,i}}{dt}$ ($\text{m}^{-3} \text{s}^{-1}$) is the change in particle number concentration over time in box k for size bin i . NF represents the near field and FF represents the far field zone relative to

the emission source (see Fig. 3). k assumes values, such as NF, FF1, FF2, *etc.*, depending on the chosen room geometry.

$J_{\text{source},k,i}$ is a single point NM generation term, assumed to be at the center of the NF box:

$$J_{\text{source},k,i} = 0 \text{ if } k \neq \text{NF and } J_{\text{source},k,i} = \frac{S_i}{V_{\text{NF}}} \text{ if } k = \text{NF} \quad (2)$$

where S_i (s^{-1}) is the source strength estimated from measurements, or simulated using a fixed lognormal particle size distribution emission rate. In the latter case, the emission rate, n , is calculated as a function of N (m^{-3}), the total number concentration of the particle distribution, σ_G , the geometrical standard deviation of the distribution, and μ_G (nm), the geometric mean diameter of the distribution:

$$n(D_p) = N \frac{1}{\log(\sigma_G)\sqrt{2\pi}} \exp\left\{\frac{-[\log(D_p/\mu_G)]^2}{2[\log(\sigma_G)]^2}\right\} \quad (3)$$

In eqn (3), D_p is the defined bin diameters of the NM size distribution. In eqn (2), V_{NF} (m^3) is the volume of the NF box.

$J_{\text{exchange},k,i}$ is the transport between the k th box and its connected boxes. It is the main driver for the transport processes for the size bin i (in $\text{m}^{-3} \text{s}^{-1}$) in the system:

$$J_{\text{exchange},k,i} = \frac{1}{V_k} \sum_l (Q_{lk}N_{l,i} - Q_{kl}N_{k,i}) \quad (4)$$

where l is a different box in the indoor environment as defined by the geometry or is an inlet or exhaust, V_k (m^3) is the volume of the box l , and Q_{kl} is the air flow rate ($\text{m}^3 \text{s}^{-1}$) from box k to box l , positive or zero, by definition. This equation also encompasses the introduction or removal of particles from the system by the general room ventilation inlet and exhaust. In the case of the inlet and exhaust, the inflow concentration is generally assumed to be 0 m^{-3} if not taking the influx of particles from elsewhere into consideration.

$J_{\text{coagulation},k,i}$ is the coagulation due to Brownian collision, Brownian coagulation, and turbulent collision of particles. The number concentration change rate ($\text{m}^{-3} \text{s}^{-1}$) from the process of coagulation is determined as:

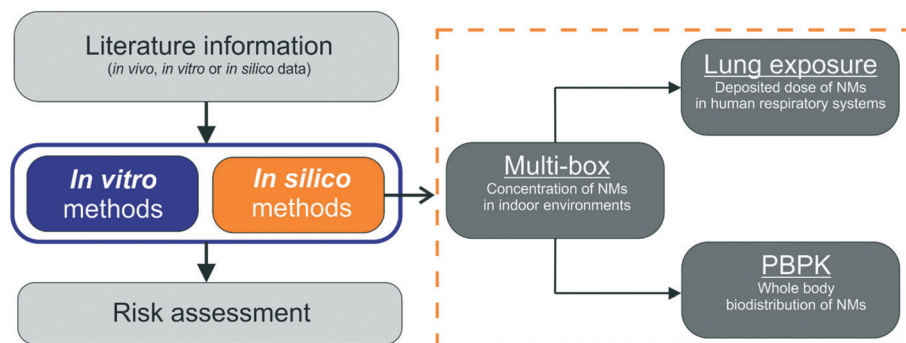


Fig. 1 Schematic of the data transfer from one module to the next in the integrated computational framework for *in silico* assessment of the inhalation of aerosolized NMs.



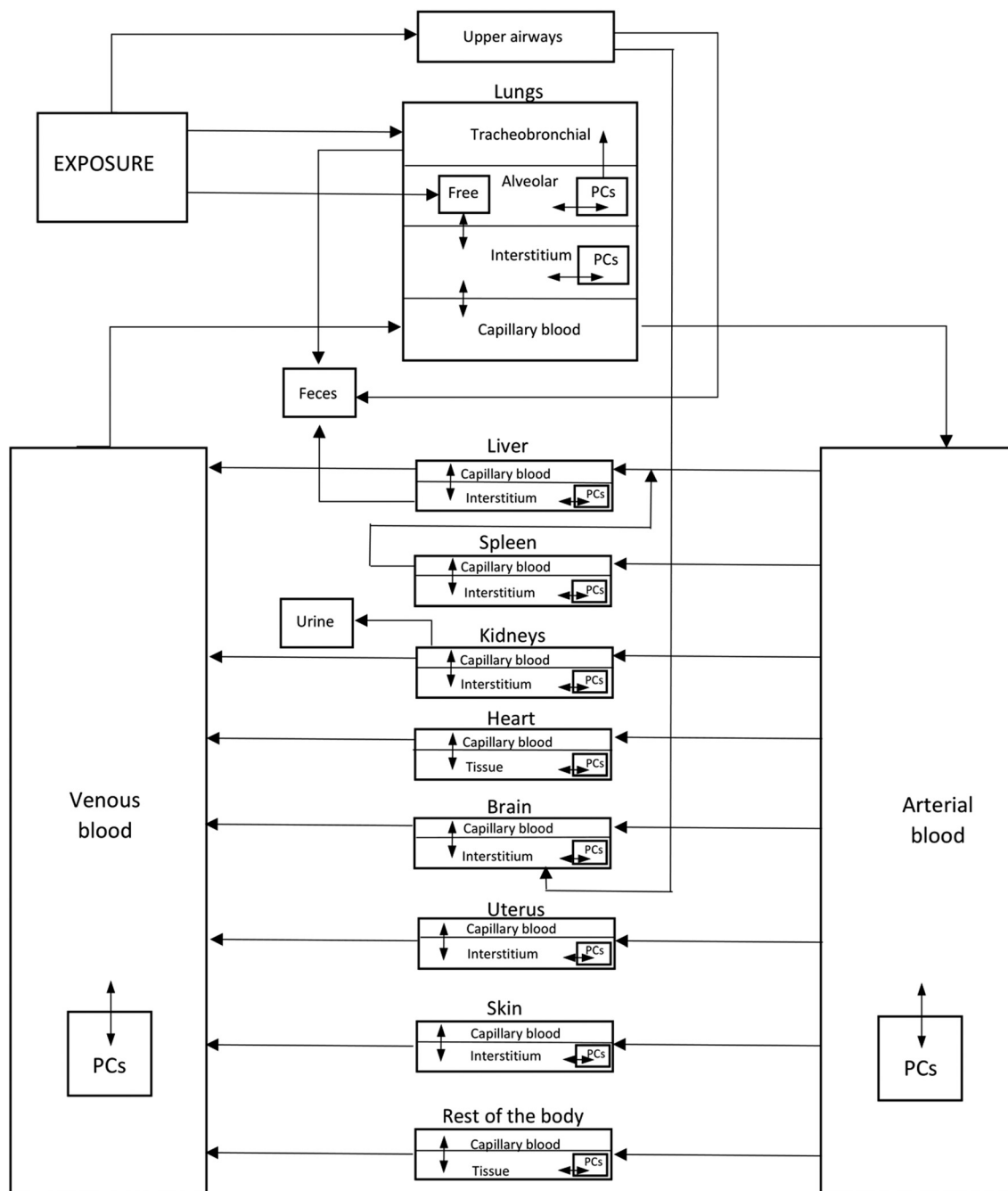


Fig. 2 Schematic representation of the structure of the TiO_2 NM PBPK model. PC stands for phagocytizing cells which take up NMs and transport them into/between model subcompartments.

$$j_{\text{coagulation},k,i} = \frac{1}{2} \sum_{j=1}^{i-1} K_{j,i-j} N_{k,j} N_{k,i-j} - N_{k,i} \sum_{j=1}^{\infty} K_{i,j} N_{k,j} \quad (5)$$

where K ($\text{m}^{-3} \text{s}^{-1}$) is the statistical coagulation coefficient between spherical particles based on Brownian collision, Brownian coagulation, and turbulent collision.²⁹ Here, coagulation removes particles of specified D_p size bins and adds the agglomerated particles to the appropriate D_p size bins in order to keep the total volume constant, assuming a sphere diameter of similar volume. When two particles

collide and are assigned to the largest size bin, the number concentration is adjusted to conserve mass.

$j_{\text{deposition},k,i}$ describes the removal of aerosol particles that adhere to surfaces in the room:

$$j_{\text{deposition},k,i} = -\frac{1}{V_k} \sum_r A_{k,r} u_{k,r,i} N_{k,i} \quad (6)$$

where A is the area (m^2) that is available for deposition in direction r , upwards, downwards, and u is the size-dependent



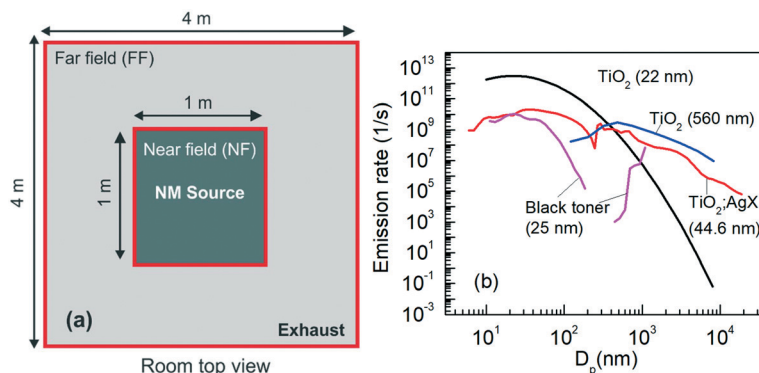


Fig. 3 (a) The computational domain, *i.e.*, the Room, indicating the near field (NF) where the source of the NMs is located and the far field (FF) where the exhaust is located. The dimensions of each area used in the integrated model are shown. (b) The size-resolved emission rate distributions of the NMs used in this work. Besides the user defined TiO_2 (22 nm), all distributions are based on experimental data.^{37,39–41}

deposition velocity (m s^{-1}). The deposition velocity was calculated according to Lai and Nazaroff.³⁰

2.2 The lung exposure model

The lung deposition model is based on a simplified version of the International Commission on Radiological Protection (ICRP) model.³¹ The ICRP model was initially developed for estimation of the deposition dose to organs and tissues resulting from the inhalation of radioactive particles, and uses empirical equations based on experimental data and theory to estimate the deposition dose in various regions of the human respiratory system. The developed lung deposition model focuses on three regions, namely alveolar (AL), tracheobronchial (TB) and head airways (HA). The model equations for the deposited dose in the AL (eqn (7)), TB (eqn (8)) and HA (eqn (9)) regions are:

$$DF_{\text{AL}} = \left(\frac{0.0155}{D_p}\right) \left\{ \exp\left[-0.416(\ln(D_p) + 2.84)^2\right] + 19.11 \exp\left[-0.482(\ln(D_p) - 1.362)^2\right] \right\} \quad (7)$$

$$DF_{\text{TB}} = \left(\frac{0.0352}{D_p}\right) \left\{ \exp\left[-0.234(\ln(D_p) + 3.40)^2\right] + 63.9 \exp\left[-0.819(\ln(D_p) - 1.61)^2\right] \right\} \quad (8)$$

$$DF_{\text{HA}} = \text{IF} \left\{ \frac{1}{1 + \exp[6.84 + 1.183 \ln(D_p)]} + \frac{1}{1 + \exp[0.924 - 1.885 \ln(D_p)]} \right\} \quad (9)$$

where:

$$\text{IF} = 1 - 0.5 \left(1 - \frac{1}{1 + 0.00076 D_p^{2.8}} \right) \quad (10)$$

is the inhalable fraction (IF). Eqn (7) and (8) consider the IF implicitly, since they are fitted to data that include the effect of inhalability. The deposited dose fraction as a function of particle size, D_p , is shown in Fig. S1,† along with the geometric mean diameter (GMD) of the NM emissions used in this work.

In order to calculate the dose, the mass size distribution is calculated from the NM number size

distribution, assuming spherical particles and a NM density, d (eqn (11)):

$$m_i = 1/6\pi D_{p,i}^3 d \quad (11)$$

where i refers to the different size bins. The NM mass, M_x , deposited at timepoint t as a result of the particle concentration in the defined box reads:

$$M_{x(x=\text{AL,TB,HA}),t} = \sum_i (m_i C_{\text{NMs},i,t} DF_{x,(x=\text{AL,TB,HA}),i}) \quad (12)$$

where C_{NMs} is the NMs concentration coming from the multi-box aerosol model. The deposited doses in the three lung regions (AL, TB and HA) are computed as the sum of the product of $M_{x,(x=\text{AL,TB,HA}),t}$ with the respiratory volume (V_r), and time between each time point for the simulation, Δt_{expo} , given as:

$$\text{DOSE}_{x,(x=\text{AL,TB,HA})} = \sum_t M_{x,(x=\text{AL,TB,HA}),t} \Delta t_{\text{expo}} \quad (13)$$

2.3 PBPK model for inhalation exposure to TiO_2 NMs

The PBPK model developed herein to describe the biodistribution of TiO_2 NMs after inhalation is based on the structural model presented in ref. 32. Inhalation is considered as the main risk-relevant exposure route in occupational settings, since the amount of particles reaching the systemic circulation through skin penetration can be considered negligible.^{32,33} Initially, a PBPK model was developed for rats and was then extrapolated to humans. The



parameters of the model were recalibrated using the biodistribution data produced by Kreyling *et al.*,³⁴ in which 20 adult Wistar Kyoto rats were divided into 5 groups and exposed to slightly different doses of ⁴⁸V-radiolabeled 20 nm TiO₂ NM aerosol for 2 hours *via* an endotracheal tube. Each group was exsanguinated and dissected to extract biodistribution data and the quantities of TiO₂ NMs in specific tissues were calculated indirectly using ⁴⁸V radioactivity, measured with γ -spectrometry, which was then matched to TiO₂ through mass and radioactivity balances. The first rat group was sacrificed immediately after exposure, and then the second, third, fourth and fifth groups were euthanized 4 hours, 24 hours, 7 days and 28 days post exposure, respectively.

The tissue compartments for which measurements were reported were the total lungs, lavaged lungs, bronchoalveolar lavage cells (BALC), which refers to cells retrieved from the broncho-alveolar lavage procedure, bronchoalveolar lavage fluid (BALF), *i.e.*, free TiO₂ NMs in the BALF, trachea, liver, spleen, kidneys, heart, brain, uterus, blood, carcass, skeleton, soft tissue, secondary organs and skin. From those, total lungs, skeleton, soft tissues and secondary organs were not used since they included biodistribution information from combinations of other compartments. With regard to excreta, cumulative faeces and urine data were drawn from the respective plots provided in ref. 35 for the 28 days rat group.

The structural model was mostly guided by the compartments for which biodistribution data were available.³⁴ The most significant compartments were the trachea, BALF, BALC and lavaged lungs. The nature of the exposure is such that most NMs were either deposited in the lung region or excreted, whereas only a small amount were translocated across the air-blood-barrier into the systemic circulation.³⁴ The lung biodistribution is expressed through 4 compartments, one for the tracheobronchial region, one for the alveolar region, one for the interstitium and one for the capillary blood of the lungs. In the first two compartments the NMs exist in a “free” state, while in the alveolar and interstitium regions the NMs can be endocytosed by macrophages which are phagocytizing cells (PCs). In relation to the rest of the tissues, three sub-compartments were considered, one for the capillary blood, one for the tissue interstitium and a compartment for phagocytosis by tissue resident PCs. The capillary blood exchanges NMs with the interstitium compartment, which is also in contact with the PCs sub-compartment.

The TiO₂ NMs enter the system *via* three compartments, namely the tracheobronchial region, the alveolar region and the upper airways. Apart from the respiratory tract, the rat PBPK model contains two blood pools, the arterial and venous, and 8 tissue compartments, namely the liver, spleen, kidneys, heart, brain, uterus, skin and rest of the body, which incorporates all remaining tissues that have not been stated explicitly. Excretion of the NMs takes place *via* three compartments: (a) in the liver, through hepatobiliary excretion from the liver tissue to faeces, (b) in the kidneys,

where NMs are excreted to urine, and (c) through tracheobronchial clearance. The schematic presentation of the developed PBPK model is illustrated in Fig. 2. The model includes a number of physiological (organism-specific) and substance-specific parameters. Organism-specific parameters are the regional blood flows, tissue volumes, volumes of vascular and interstitial spaces, the inhalation volume and rate, and the typical number of PCs in each organ. Regarding the substance specific parameters, these include the deposition fractions, tissue permeability coefficients, tissue: blood partition coefficients, the maximum uptake rates by PCs, the maximum uptake capacity of PCs, the release rate of NMs from PCs, the clearance rates and, finally, the various transfer rates in the respiratory system. The PBPK model equations are presented in section 1 of the ESI† file.

After defining the structural model, the next step was to integrate the information contained in the data with prior information found in the literature regarding the parameters of the ordinary differential equations system. This was performed using a dynamic form of the Hamiltonian Monte Carlo (HMC) algorithm, the No-U-Turn Sampler.³⁵ Prior literature knowledge in the form of distributions was drawn from ref. 32 and 36. The statistical model is described in more detail in ref. 37.

After building the rat model, a simple extrapolation approach was followed to acquire a human TiO₂ NM inhalation PBPK model. The first extrapolation step involved the replacement of the rat physiological parameters with those of the human. Thiel *et al.*³⁸ showed that scaling of the physiological parameters was the most efficient univariate change when conducting cross-species extrapolation for a series of drug compounds. Due to the lack of human biokinetic data, the kinetic substance-specific parameters, *i.e.*, clearances, transfer rates, uptake rates *etc.*, could not be precisely extrapolated. Therefore, those parameters were scaled using allometric scaling.³⁶ The parameters of the rat and human models are presented in Tables S1–S4.†

2.4 Computational specifications for integration of the 3 models

The computational framework consists of three parts. The first part is the multi-box aerosol application which is used to compute the concentrations of the NMs in the closed environment, namely the Room. A two-box layout is used, *i.e.*, the Room is partitioned into two areas, an NF area in which the source of the NMs is located and a FF area where the exhaust of the system is located (see Fig. 3a). The Room size is $4 \times 4 \times 4 \text{ m}^3$ which is a common working room size. The NF size is $1 \times 1 \times 1 \text{ m}^3$. A two box layout is selected since this provides the most accurate results while maintaining the computational cost at reasonable levels.¹¹ The flow rate between NF and FF is set to $10 \text{ m}^3 \text{ min}^{-1}$ and the exhaust flow rate is set to $5 \text{ m}^3 \text{ min}^{-1}$, similar to the values used in ref. 10 and 11. A parametric analysis of the input values and their impact on the overall computational outputs is the subject of a forthcoming publication.



The initial D_p distributions of the four NMs used in this work are shown in Fig. 3b, namely carbon black (black toner) with a GMD of 25 nm, TiO₂ with a GMD of 560 nm, TiO₂:AgX particles with a GMD of 44.6 nm and a user defined distribution which corresponds to TiO₂ with a geometric average diameter of 22 nm. TiO₂ (22 nm) is theoretically constructed *via* eqn (3) with $N = 2.5 \times 10^{12}$, $\sigma_G = 2.1$ and $\mu_G = 22$ nm. The emission rate, n , is chosen so that a realistic occupational exposure scenario is generated. Specifically, the average NM concentration in the NF using the selected n value results in a time weighted average (TWA) of around 5.8 mg m⁻³ for the NF and 3.9 mg m⁻³ for the FF for an 8 hours work shift. These values have a regulatory relevance, since the US National Institute for Occupational Safety and Health (NIOSH) has suggested that for TiO₂ NMs a value of 0.3 mg m⁻³ is the recommended exposure limit (REL) over a 10 hours workday and 40 hours week,⁴² while 1.2 mg m⁻³ has been proposed by the Japanese Industrial Technology Development Organization (NEDO).⁴³ The occupational exposure scenarios for comparing the NMs deposition data generated from the lung exposure and the PBPK model utilised the 22 nm TiO₂ NMs, as the PBPK model was constructed using biodistribution data referring to 22 nm TiO₂ and, thus, the PBPK simulations for TiO₂ NMs with similar diameter are considered to be the most credible currently.

The lung exposure and PBPK applications take as input the NM concentrations from each exposure area (room) and compute the deposited dose of the NMs in the various regions of the human respiratory system (and throughout the body in the case of the PBPK model). Using eqn (3), a theoretical lognormal particle size distribution is generated based on 30 size bins. Using the NM density, the particle concentration is converted into mass concentration, which is then provided as input to the two models. Following that, the two models calculate the deposited mass per bin for each lung region, and the deposited mass summation of all bins for each region is the final reported product. All exposure simulations refer to spherical particles.

The lung exposure application can compute the deposited dose in the alveolar, head airways and tracheobronchial regions, while the PBPK application, besides the aforementioned regions, offers the ability to simulate the resulting biodistribution in the organs of the systemic circulation, *i.e.*, the translocation of the NMs through the air-lung barrier. The inhalation rates used as inputs to the lung exposure and PBPK models in order to simulate different inhalation conditions are shown in Table 1.

Although all three model applications are independent, the lung exposure and PBPK applications have an embedded

Table 1 Inhalation rate in L min⁻¹ (ref. 24) per gender and physical activity level

	Female	Male
Sitting	6.5	9
Light exercise	20.8	25
Heavy exercise	45	50

module allowing the generation of NM concentration-time profiles using the multi-box aerosol model, but also give to the user the ability to provide custom-made occupational exposure scenarios. All applications are freely available and can be found at:

Multi-box aerosol application: <https://aerosol.cloud.nanosolveit.eu/>

Lung exposure: <https://lungexposure.cloud.nanosolveit.eu/>

PBPK: <https://exposurepbpk.cloud.nanosolveit.eu/>

These web applications are offered to the community through the NanoSolveIT⁴⁴ cloud platform (<https://cloud.nanosolveit.eu/>) and contribute to implementation of a comprehensive nanoinformatics-driven decision-support strategy that promotes nanosafety based on innovative *in silico* methods, models and tools, while reducing reliance on animal testing, which is the major goal of the project. Presenting the developed nanoinformatics tools as freely available, user-friendly web applications accompanied by appropriate model documentation and user guides significantly increases model accessibility and usage, even by non-experts. Enhanced understanding, utilization and acceptance of nanoinformatics tools can bridge the gap between nanosafety-related regulators and industry, thus accelerating the industrial and commercial exploitation of nanomaterials in a variety of consumer applications, whilst minimising their environmental and human health impacts.

3. Results

Given that no human *in vivo* data are available for validating the models, we compare the results obtained from the lung exposure and the PBPK model with the output of the multiple-path particle dosimetry (MPPD) model,⁴⁵ which is considered the gold standard in the calculation of particle deposition in the respiratory system. Then, the deposited doses reported by the two models are compared against each other for different time intervals, room regions, exercise levels and sexes. This comparison aims at exploring the effect of NM clearance and translocation from the lung into the blood circulation, which are included in the PBPK model but not in the lung exposure model, on the exposure dose, and thus the likely effects over time, which future iterations of our IATA will also incorporate. Finally, additional simulations are performed using the lung exposure model in order to estimate the deposited dose of various NMs in the NF and FF areas of the computational domain.

3.1 Comparison of the models with MPPD in the TiO₂ NM case

The lung exposure, PBPK and MPPD applications were used to collect and compare biodistribution simulation results, regarding exposure of female and male workers to 22 nm TiO₂ NMs, under light exercise as part of an 8 hours work shift (Fig. 4). The MPPD does not include an option for providing a detailed exposure time series, but only allows for an hourly variation of the external concentration, and, thus, a steady concentration equal to 5.85 mg m⁻³ was used in all three models. Additionally, the Yeh/Schum symmetric lung



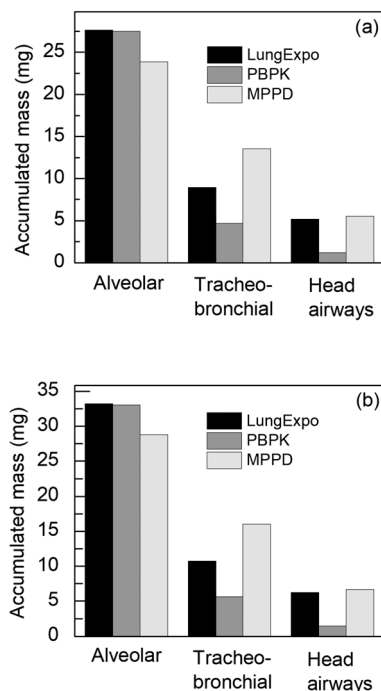


Fig. 4 Comparison of the accumulated mass of TiO_2 NMs in the three different lung regions determined using the lung exposure, PBPK and MPPD models for (a) female and (b) male humans under light exercise level physical activity during occupational exposure for 8 hours to 22 nm TiO_2 NMs.

deposition model was used for the MPPD calculations.⁴⁶ Since deposition eqn (7)–(9) refer to nose breathing, the same breathing route was considered for the MPPD model. Regarding inhalation and lung parameters, all models used the same values to ensure that any differences between them are related to the underlying model. The input data provided to the MPPD are presented in Table S5.†

The slight differences in the deposited mass between the lung exposure application and the MPPD arise from differences in the deposition fractions. Specifically, in the lung exposure application the deposited mass in the alveolar region is slightly greater than that recorded by the MPPD model, while the reverse behaviour is applied to the head airways. The two models estimate a similar deposited mass for the tracheobronchial region. The greater differences between the deposited mass of these two models and the PBPK model in the alveolar and head airways regions are due to the pulmonary clearance terms included in the PBPK model, *i.e.*, tracheobronchial and head airways NM clearance, and the translocation of NMs from the lung into the systemic circulation, which are initiated as soon as the first particles are deposited in the respiratory system.

3.2 Lung exposure versus PBPK model performance in the TiO_2 NMs case – effect of clearance

The effect of clearance on the final deposited dose was investigated *via* a series of *in silico* experiments, in which the

22 nm TiO_2 NMs were used. Two scenarios were considered; a short term exposure lasting 600 seconds and a long term one, which represented a full 8 hours working day *i.e.*, 28 800 seconds. In the first case the source was active for the first 300 seconds. For the working day, the simulation time was partitioned into 16 timesteps of 1800 seconds (30 minutes) each with the source being active for the first 900 seconds of each step. The evolution of the average NM concentration, over the D_p distribution, for the NF (*i.e.*, close to the NMs source where the worker is performing the handling operation) is shown in Fig. 5.

Fig. 6 presents the TiO_2 NM deposited doses after 600 s of exposure in the NF and FF areas, respectively, for both female and male workers under different exercise levels. As expected, the accumulated mass decreases as we move from the NF, where the source of the NMs is located, to the FF, where the exhaust is located, and increases from sitting to heavy exercise. Male workers register the largest amount of accumulated mass during heavy exercise, due to the higher underlying inhalation rate. In all cases, the alveolar region records the largest amount of accumulated particle mass followed by the tracheobronchial and the head airways regions respectively, in terms of the estimated deposition fractions obtained from the Hinds' equations for the particular particle diameter (Fig. S1†).

Comparison of the lung exposure and PBPK models under the short-term exposure scenario case (Fig. 6) reveals small differences in terms of the computed accumulated NM

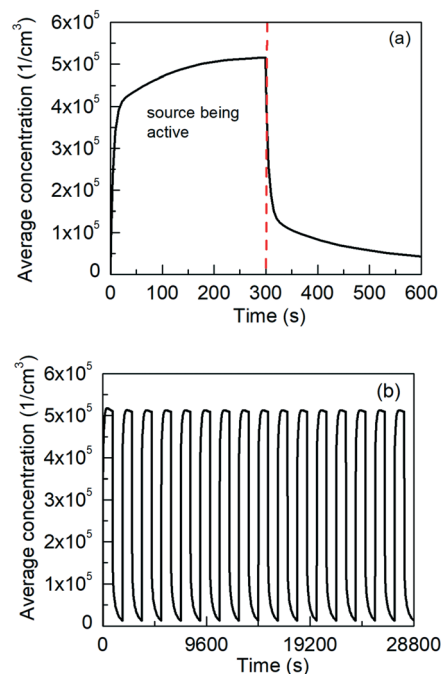


Fig. 5 Average concentration evolution of TiO_2 NMs (22 nm) in the NF for (a) 600 s simulation time with the source being active for the first 300 s, and (b) over the working day (28 800 s equivalent to 8 h) of simulation time. In (b) the simulation time is partitioned into 16 timesteps of 1800 s (30 min) each with the source being active for the first 900 s (15 min) of each step.



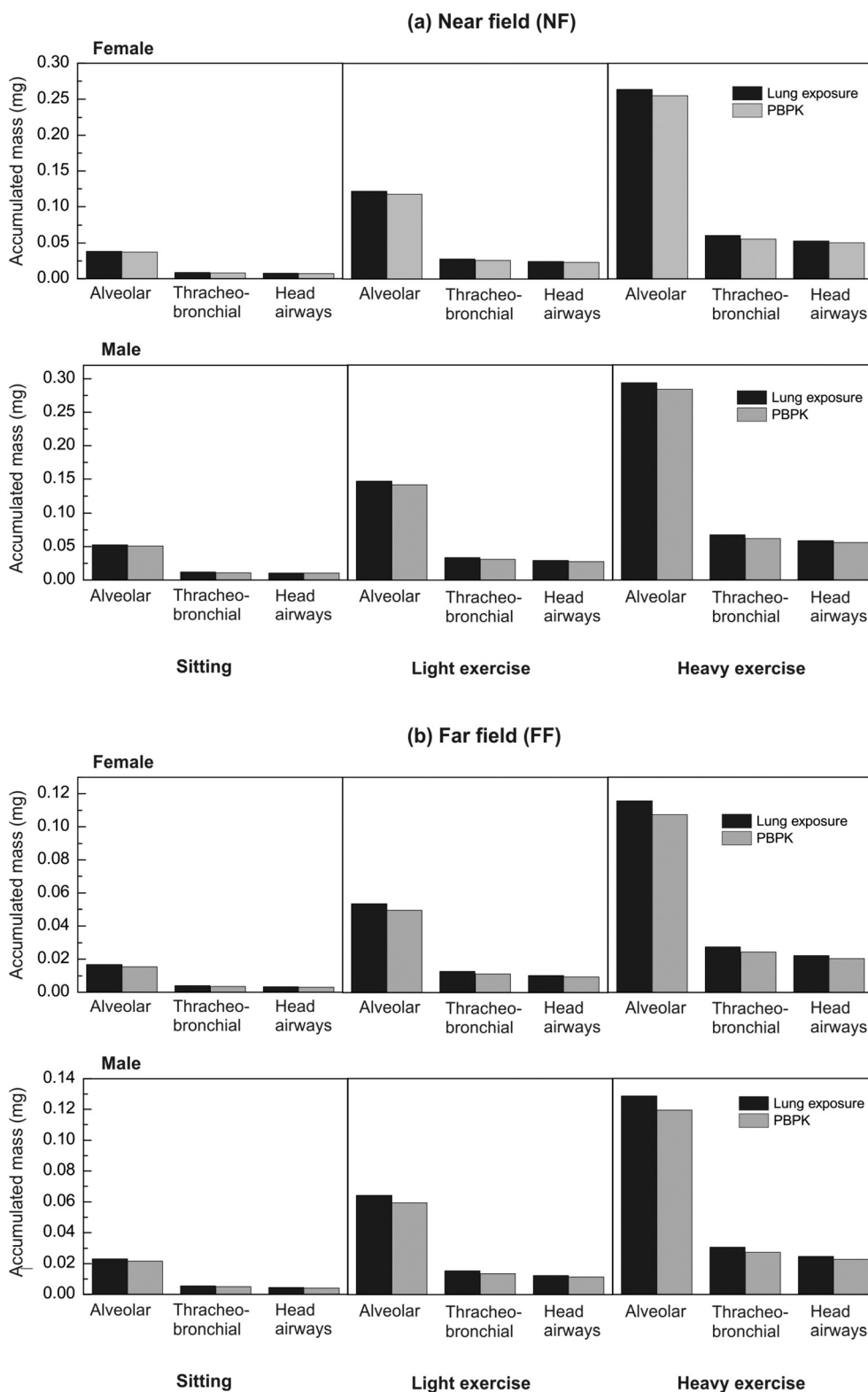


Fig. 6 Accumulated mass of the particles from the TiO_2 NMs (22 nm) emission computed for 600 s by the lung exposure and PBPK models for female and male workers under different inhalation conditions (sitting, light exercise and heavy exercise) in the (a) NF and (b) FF areas.

masses. This is an expected result, because the two models use the same equations for estimating the deposition in the various respiratory regions. Furthermore, the exposure

duration is too short compared with the clearance kinetics of the PBPK model to result in substantially reduced accumulated TiO_2 mass over short exposure times.



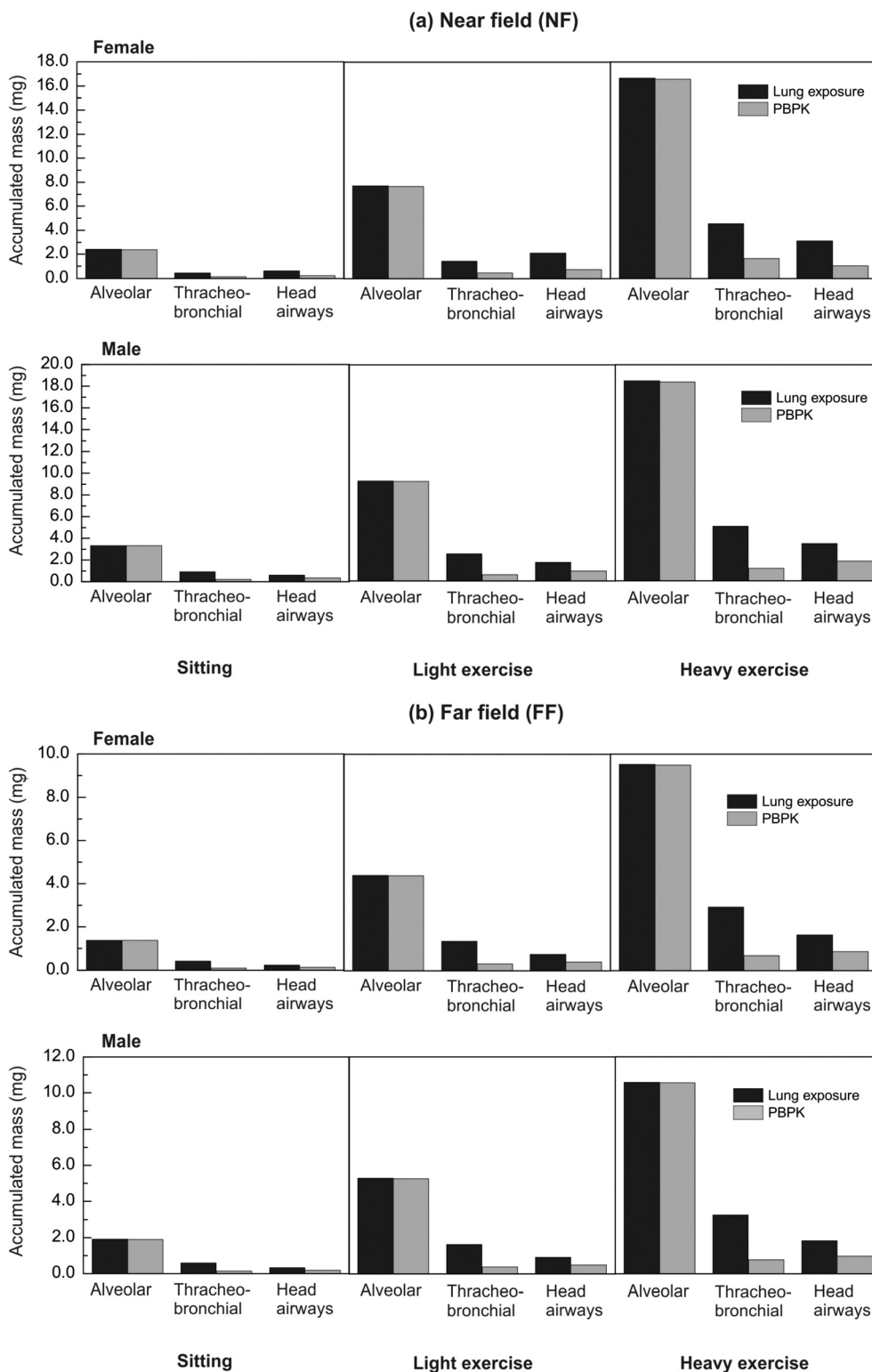


Fig. 7 Accumulated mass of particles from the TiO_2 NMs (22 nm) emission scenario computed for a working day (8 h) by the lung exposure and PBPK models for female and male workers under different inhalation conditions (sitting, light exercise and heavy exercise) in the (a) NF and (b) FF areas.

Fig. 7 presents the computed accumulated mass over a full working day in both the NF and FF areas. In this case the exposure duration is long enough for evident alterations in the final deposited mass estimated by the two models to be

recorded. In the alveolar region, the clearance term of the PBPK model is slow, since it refers to long term clearance mediated by macrophages (phagocytosing cells as shown in Fig. 2), and the final accumulated mass is not affected



significantly by it, as in the short-term exposure case. On the other hand, the clearance from the tracheobronchial and the head airways regions, which directs trapped NMs to the gastrointestinal tract, is fast enough that the decrease in the accumulated mass is important.

To further explore the effect of clearance on the accumulated NM mass we performed simulations for a longer duration using the PBPK model. Specifically, the same 8 hours exposure for a female worker under heavy exercise load in the NF was used as input and the model simulated the evolution of the biodistribution for an extra 98 hours (100 hours of total simulation time). The results are presented in Fig. 8 and illustrate that the alveolar clearance by phagocytizing cells is slow, meaning that the TiO₂ mass accumulates in the alveolar region. The tracheobronchial clearance is fast for the first 40 h leading to a rapid decrease in the accumulated mass, but after 40 h, the accumulated mass decreases at a much slower rate. Finally, the clearance of the head airways is fast, meaning that all of the TiO₂ dose is removed within 50 h.

3.3 Accumulated mass computations for other NMs

Since the PBPK model does not currently support other NMs besides TiO₂, we employed the lung exposure model to compute the accumulated mass of the other NMs, *i.e.*, TiO₂:AgX (44.6 nm), TiO₂ (460 nm) and carbon black from toner (25 nm), for a working day, using the exposure scenario described previously (8 h exposure, split into 16 segments of 30 minutes with the NMs source active for the first 15 minutes of each time segment) using the particle emission rates shown in Fig. 3b. The results are shown in Fig. S2–S4.† As in the case of the TiO₂ NMs (22 nm), the accumulated mass of all NMs decreases as we move from NF to FF and increases from sitting to heavy exercise.

Fig. S2–S4† show that most of the particle mass is deposited in the head airways. While the TiO₂ (22 nm) distribution was constructed using eqn (3), the distributions of the other NMs were derived from experimental data meaning that background particles or other aerosol dynamic effects, such as *e.g.*, aggregation and agglomeration, may

influence the measured particle number size distributions and thus the calculated size-resolved emission rates. In the case of TiO₂ (560 nm), sanding fragments containing nanosized TiO₂ were measured.

From the materials studied, the maximum accumulated mass is 1148.5 mg and is observed in the head airways for TiO₂ (560 nm), for male workers during heavy exercise located in the NF, which corresponds to approximately 2.8×10^{17} TiO₂ particles of different sizes according to the experimentally derived size distribution. In terms of maximum accumulated particle number, the same scenario, *i.e.*, male workers during heavy exercise in the NF, TiO₂:AgX yields the highest deposition in the head airways, with roughly 1.85×10^{18} particles (see Fig. 9). This outcome is

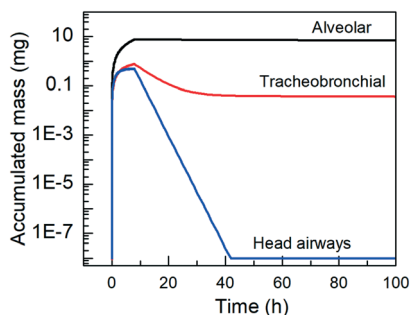


Fig. 8 Evolution of the accumulated TiO₂ NM (22 nm) mass over 100 hours following 8 hours of exposure of a female worker under heavy exercise conditions in the NF predicted using the human PBPK model.

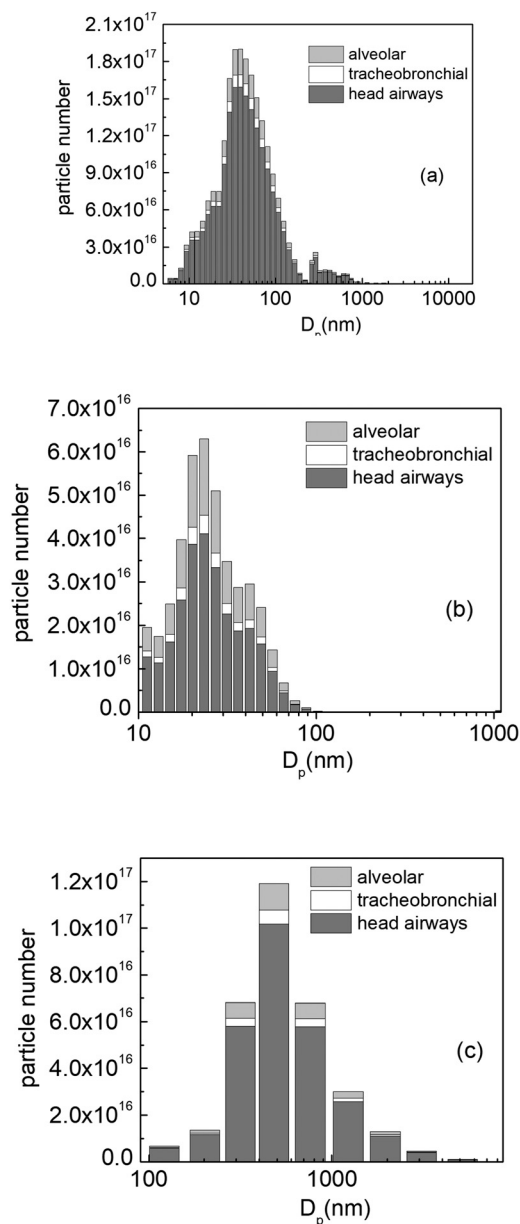


Fig. 9 Particle number distribution for (a) TiO₂:AgX, (b) black tonner and (c) TiO₂.



expected since NMs with bigger particle sizes have lower particle numbers in equivalent mass.

To understand the impact of the variance of the size distribution on the deposited dose, we introduce an example using the distribution of TiO₂:AgX (44.6 nm), with the analysis holding for all other NMs. The value of σ_G (unitless), the geometrical standard deviation of the particle size distribution, for the experimental distribution of TiO₂:AgX (44.6 nm) is 2.5. Using eqn (3), we constructed two alternative distributions with $\sigma_G = 2.1$ and 1.5 (Fig. 10a). The computed accumulated NM masses are shown in Fig. 10b for a female worker during light exercise in the NF area. The results are normalized against the maximum deposited mass in each case, in order to avoid comparability issues, since the accumulated mass varies significantly in each case. As expected, as σ_G decreases and the distribution becomes narrower around the geometric mean, the ratios of the accumulated NMs masses come into line with the deposition fraction calculated according to Hinds' equation for a particle with a GMD of 44.6 nm. In other words, for similar GMDs, the greater the σ_G the higher the deposition in the head airways regions.

3.4 Which model provides the optimal predictions for RA and LCIA?

Two *in silico* approaches for assessing the deposition of NMs in the human respiratory system in an occupational setting are presented, namely the multi-box aerosol model coupled with the lung exposure model and the integration of the multi-box aerosol model with a PBPK model, which form the basis for next generation risk assessment through *in silico* determination of exposure and consequent human health. At first glance, there seems to be a significant overlap between the two approaches, because both models use the same empirical equations for deriving the deposition fractions. However, the PBPK model includes additional equations to describe in a more holistic manner the biodistribution of TiO₂ NMs in the human body after inhalation exposure, which allows simulation of long-term exposure scenarios with more accurate results. Still, the derivation of a PBPK model is a demanding task and requires a comprehensive set of experimental data, such that PBPK models are currently

limited to only a handful of NMs, as in the present work for the case of TiO₂ NMs. On the other hand, the lung exposure model can calculate the deposited NM mass only in the head airways, alveolar and tracheobronchial regions but for any NM where the inhaled size distribution is known.

A weakness of the lung exposure model covered by the PBPK model is the absence of systemic clearance. Therefore, using the lung exposure model under acute exposure scenarios can lead to safe results regarding the deposited mass of NMs in the respiratory system. For longer exposure durations, be it a working day, week, month or year, using the lung exposure model can induce notable overestimations in the calculated mass accumulation, which for precautionary reasons in the context of risk assessment for human health may be beneficial. Thus, the lung exposure application can provide an upper limit for the deposited dose resulting from occupational exposure scenarios to varying concentrations of a NM with a known size distribution, in the absence of more complex mechanistic models.

The deposited mass estimated by both models was similar to the one reported by the MPPD. MPPD is a robust tool that includes a multitude of mechanistic models for estimating the deposition of a wide variety of materials under different exposure scenarios. However, one of its major drawbacks is that it doesn't offer the ability to provide complex concentration-time profiles. This makes it a tool that is more suited to controlled experimental conditions rather than occupational exposure scenarios stemming from complex industrial applications. The lung exposure and PBPK applications fill this gap, allowing for deposition estimation of complex, real-world applications.

Fig. 11 introduces the proposed framework for lung internal deposition prediction. If the spatiotemporal evolution of the concentration of the NM is not known, then it can be estimated using the multi-box aerosol model. The concentration-time profile can then be parsed as input to one of the two biodistribution models. If the exposure is of acute nature, *e.g.*, the result of an accident, then the lung exposure model can be used to estimate the deposited mass in the respiratory system without significant loss of precision due to the absence of clearance mechanisms. The PBPK model is a better tool for estimation of mass deposition following a

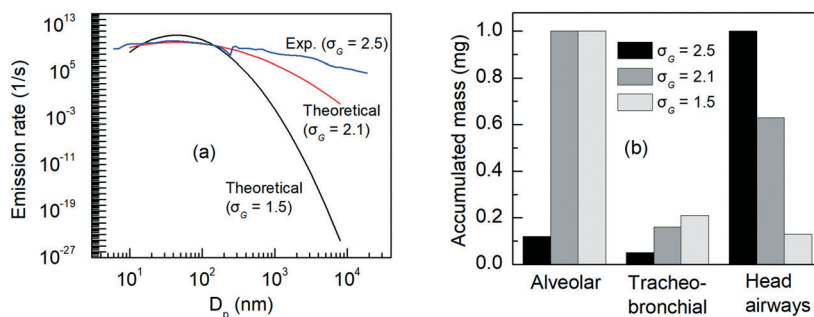


Fig. 10 TiO₂:AgX (44.6 nm) (a) distributions and (b) computed accumulated mass for $\sigma_G = 2.5, 2.1$ and 1.5 for a female undertaking light exercise in the NF area over an 8 h working day.



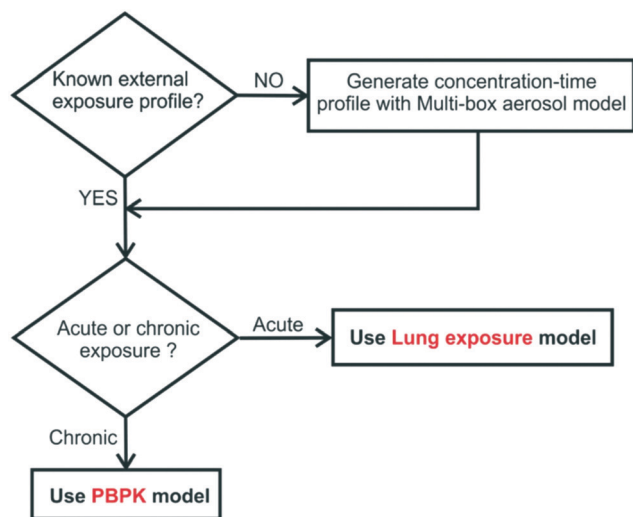


Fig. 11 Proposed framework for NMs internal deposition prediction, depending on the available input information.

chronic exposure. It has to be noted that so far, the PBPK model can be used for assessing the internal exposure of TiO₂ (preferably around 22 nm) NMs, but can be extended to include more NMs as *in vivo* data become available or as read-across models increase in power. The lung exposure model can be used for exposure to TiO₂, TiO₂:AgX, black tonner and carbon black, but can also be used for any NM provided that the particle size distribution emission rate is known.

The underlying goal of deposition prediction is to link it with the toxicity of the material. For conventional chemicals, toxicity is directly related to the amount of administered material, so the most common dose metric in the case of inhalation is the total deposited mass. In the case of NMs, chemical composition is not the only driver of toxicity, with other factors, *e.g.*, NM size, playing an important role as well. Therefore, administered mass alone is not sufficient as a metric to account for the toxicity of a NM, so depending on the exposure conditions, route, NM *etc.*, different dose metrics such as particle number, particle volume or surface area should be examined.⁴⁷ For instance, Braakhuis *et al.*⁴⁸ concluded that in the case of pulmonary inflammation due to inhalation exposure to silver NMs, the appropriate dose metric is the particle surface area in the alveoli. The tools developed in this work report the final deposited mass in three regions of the respiratory system after inhalation exposure, but can be extended to report different dose metrics, *e.g.*, particle number as illustrated in the previous section, or an even more advanced output with particle number per size bin.

The natural next step for enabling risk characterization of occupational inhalation exposure to NMs is the inclusion of hazard values as a toxicity metric related to the NM exposure. For human health risk assessment, the derived no-effect level (DNEL) or occupational exposure limit (OEL) are used to derive the maximum levels of exposure to a chemical that humans should be exposed to. These values can be combined

with the results of the models presented here to form the risk characterization ratio (RCR), with the exposure estimator as the numerator and the DNEL or OEL as the denominator. The risk to humans can be considered acceptable if the estimated exposure levels do not exceed the hazard values, *i.e.*, if RCR < 1.

Unfortunately, due to the multitude of NMs and the range of their toxicological responses, such hazard values are rarely found in literature. Using *in vivo* dose–response data, the benchmark dose (BMD) approach^{49–51} can be used to derive the point of departure (POD), also known as a reference point, which is the dose above which adverse effects start to emerge. Dividing the POD by a series of appropriate uncertainty factors can produce the corresponding DNEL. An alternative approach is to estimate the hazard values using predictive modelling. More precisely, nano-Quantitative-Structure–Activity-Relationship (nanoQSAR)^{52,53} models can build a mapping from the structure and physicochemical characteristics of the NMs to the desired response, in this case the hazard values, utilizing data-rich NMs to make predictions about data-poor ones.

Finally, the output of the deposition model could be linked to relevant adverse outcome pathways (AOPs),⁵⁴ a tool in toxicology and risk assessment for representing biological knowledge spanning multiple biological levels. The AOP links a biological perturbation caused by a stressor through the molecular initiating event to an adverse outcome through a series of key events.

Several NMs-specific AOPs have already been proposed, including a putative AOP for lung fibrosis, in which high exposure, in terms of mass, duration or both, leads to loss of tissue elasticity and reduced lung function and the resulting chronic inflammation is also linked to onset of cancer and other diseases.⁵⁵ More recently, a putative AOP for deposition and retention of NMs in the lung leading to cancer has been proposed that includes *in silico* prediction of lung deposited dose.⁵⁶ The latter example demonstrates how tools for predicting mass deposition in the respiratory system can be linked to AOPs.

4. Conclusion

The presented framework illustrates two different approaches to predict the internal deposition and distribution of NMs following inhalation exposure in an occupational exposure setting. The developed tools have been presented as ready-to-use, well-documented web applications, to support risk-free use of NMs in the near future. In this direction, the integration of hazard values for different NMs along with inclusion of different personal protective equipment into the applications will enable the conduction of a complete occupational risk assessment, and assessment of the effectiveness of various risk mitigation measures as part of the risk management. Extension of the approach to develop an overall framework for assessment of environmental exposures to NMs is also underway.



Conflicts of interest

There are no conflicts to declare.

Acknowledgements

This work received funding from the European Union's Horizon 2020 research and innovation programme via NanoSolveIT Project under grant agreement number 814572.

References

- 1 F. Aznar Mollá, C. Fito-López, J. A. Heredia Alvaro and F. Huertas-López, New Tools to Support the Risk Assessment Process of Nanomaterials in the Insurance Sector, *Int. J. Environ. Res. Public Health*, 2021, **18**(13), 6985–7004.
- 2 G. Chen, W. Peijnenburg, Y. Xiao and M. G. Vijver, Current Knowledge on the Use of Computational Toxicology in Hazard Assessment of Metallic Engineered Nanomaterials, *Int. J. Mol. Sci.*, 2017, **18**(7), 1504–1524.
- 3 H. J. P. Marvin, Y. Bouzembrak, E. M. Janssen, M. van der Zande, F. Murphy and B. Sheehan, *et al.*, Application of Bayesian networks for hazard ranking of nanomaterials to support human health risk assessment, *Nanotoxicology*, 2017, **11**(1), 123–133.
- 4 C. Oksel, C. Y. Ma and X. Z. Wang, Structure-activity Relationship Models for Hazard Assessment and Risk Management of Engineered Nanomaterials, *New Paradigm Part Sci Technol Proc 7th World Congr Part Technol*, 2015, vol. 102, pp. 1500–1510.
- 5 J. A. J. Meesters, A. A. Koelmans, J. T. K. Quik, A. J. Hendriks and D. van de Meent, Multimedia Modeling of Engineered Nanoparticles with SimpleBox4nano: Model Definition and Evaluation, *Environ. Sci. Technol.*, 2014, **48**(10), 5726–5736.
- 6 J. A. J. Meesters, W. J. G. M. Peijnenburg, A. J. Hendriks, D. Van de Meent and J. T. K. Quik, A model sensitivity analysis to determine the most important physicochemical properties driving environmental fate and exposure of engineered nanoparticles, *Environ. Sci.: Nano*, 2019, **6**(7), 2049–2060.
- 7 M. Hauser and B. Nowack, Probabilistic modelling of nanobiomaterial release from medical applications into the environment, *Environ. Int.*, 2021, **146**, 106184.
- 8 T. Y. Sun, N. A. Bornhöft, K. Hungerbühler and B. Nowack, Dynamic Probabilistic Modeling of Environmental Emissions of Engineered Nanomaterials, *Environ. Sci. Technol.*, 2016, **50**(9), 4701–4711.
- 9 R. Hirschler, Framework for LCI modelling of releases of manufactured nanomaterials along their life cycle, *Int. J. Life Cycle Assess.*, 2014, **19**(4), 838–849.
- 10 M. P. Tsang, D. Li, K. L. Garner, A. A. Keller, S. Suh and G. W. Sonnemann, Modeling human health characterization factors for indoor nanomaterial emissions in life cycle assessment: a case-study of titanium dioxide, *Environ. Sci.: Nano*, 2017, **4**(8), 1705–1721.
- 11 A. C. Ø. Jensen, M. Dal Maso, A. J. Koivisto, E. Belut, A. Meyer-Plath and M. Van Tongeren, *et al.*, Comparison of Geometrical Layouts for a Multi-Box Aerosol Model from a Single-Chamber Dispersion Study, *Environments*, 2018, **5**(5), 52–68.
- 12 L. Xiaoping, N. Jianlei and G. Naiping, Spatial distribution of human respiratory droplet residuals and exposure risk for the co-occupant under different ventilation methods, *HVACR Res.*, 2011, **17**(4), 432–445.
- 13 Y.-S. Cheng, *Condensation Particle Counters*, In: *Aerosol Measurement [Internet]*, John Wiley & Sons, Ltd, 2011, pp. 381–392, Available from: DOI: 10.1002/9781118001684.ch17.
- 14 P. J. Drivas, P. A. Valberg, B. L. Murphy and R. Wilson, Modeling Indoor Air Exposure from Short-Term Point Source Releases, *Indoor Air*, 1996, **6**(4), 271–277.
- 15 C. Y. H. Chao and M. P. Wan, A study of the dispersion of expiratory aerosols in unidirectional downward and ceiling-return type airflows using a multiphase approach, *Indoor Air*, 2006, **16**(4), 296–312.
- 16 N. P. Gao and J. L. Niu, Modeling particle dispersion and deposition in indoor environments, *Atmos. Environ.*, 2007, **41**(18), 3862–3876.
- 17 C. Chen, W. Liu, C.-H. Lin and Q. Chen, Comparing the Markov Chain Model with the Eulerian and Lagrangian Models for Indoor Transient Particle Transport Simulations, *Aerosol Sci. Technol.*, 2015, **49**(10), 857–871.
- 18 M. A. Jayjock, T. Armstrong and M. Taylor, The Daubert standard as applied to exposure assessment modeling using the two-zone (NF/FF) model estimation of indoor air breathing zone concentration as an example, *J. Occup. Environ. Hyg.*, 2011, **8**(11), D114–D122.
- 19 E. J. Furtaw Jr, M. D. Pandian, D. R. Nelson and J. V. Behar, Modeling Indoor Air Concentrations Near Emission Sources in Imperfectly Mixed Rooms, *J. Air Waste Manage. Assoc.*, 1996, **46**(9), 861–868.
- 20 W. W. Nazaroff and G. R. Cass, Mathematical modeling of indoor aerosol dynamics, *Environ. Sci. Technol.*, 1989, **23**(2), 157–166.
- 21 J. W. Cherrie and T. Schneider, Validation of a New Method for Structured Subjective Assessment of Past Concentrations, *Ann. Occup. Hyg.*, 1999, **43**(4), 235–245.
- 22 T. Hussein, H. Korhonen, E. Herrmann, K. Hämeri, K. E. J. Lehtinen and M. Kulmala, Emission Rates Due to Indoor Activities: Indoor Aerosol Model Development, Evaluation, and Applications, *Aerosol Sci. Technol.*, 2005, **39**(11), 1111–1127.
- 23 B. Mølgaard, A.-K. Viitanen, A. Kangas, M. Huhtiniemi, S. T. Larsen and E. Vanhala, *et al.*, Exposure to airborne particles and volatile organic compounds from polyurethane molding, spray painting, lacquering, and gluing in a workshop, *Int. J. Environ. Res. Public Health*, 2015, **12**(4), 3756–3773.
- 24 J. W. Cherrie, L. Maccalman, W. Fransman, E. Tielemans, M. Tischer and M. Van Tongeren, Revisiting the effect of room size and general ventilation on the relationship between near- and far-field air concentrations, *Ann. Occup. Hyg.*, 2011, **55**(9), 1006–1015.
- 25 G. H. Ganser and P. Hewett, Models for nearly every occasion: Part II - Two box models, *J. Occup. Environ. Hyg.*, 2017, **14**(1), 58–71.
- 26 A. J. Koivisto, A. C. Ø. Jensen, M. Levin, K. I. Kling, M. D. Maso and S. H. Nielsen, *et al.*, Testing the near field/far field



- model performance for prediction of particulate matter emissions in a paint factory, *Environ. Sci.: Processes Impacts*, 2015, **17**(1), 62–73.
- 27 International Commission on Radiological Protection, *Human respiratory tract model for radiological protection: a report of a Task Group of the International Commission on Radiological Protection: adopted by the Commission in September 1993*, Pergamon Press, Oxford, 1994.
- 28 N. Cheimarios, S. Harrison, A. C. Ø. Jensen, P. Karatzas, A. Tsoumanis and P. Doganis, *et al.*, Chapter FOUR - NanoSolveIT integration of tools for assessment of human and environmental exposure to nanomaterials, In: *Handbook of Functionalized Nanomaterials [Internet]*, ed. C. Hussain and V. Kumar, Elsevier, 2021, pp. 81–120, Available from: <https://www.sciencedirect.com/science/article/pii/B9780128224151000019>.
- 29 R. Guichard, A. Tanière, E. Belut and N. Rimbart, Simulation of nanoparticle coagulation under Brownian motion and turbulence in a differential-algebraic framework: Developments and applications, *Int. J. Multiphase Flow*, 2014, **64**, 73–84.
- 30 K. Lai AC and W. W. Nazaroff, MODELING INDOOR PARTICLE DEPOSITION FROM TURBULENT FLOW ONTO SMOOTH SURFACES, *J. Aerosol Sci.*, 2000, **31**(4), 463–476.
- 31 W. C. Hinds, *Aerosol Technology: Properties, Behavior, and Measurement of Airborne Particles [Internet]*, Wiley, 1999, (A Wiley interscience publication), Available from: <https://books.google.gr/books?id=ORxSAAAAMAAJ>.
- 32 M. Senzui, T. Tamura, K. Miura, Y. Ikarashi, Y. Watanabe and M. Fujii, Study on penetration of titanium dioxide (TiO₂) nanoparticles into intact and damaged skin in vitro, *J. Toxicol. Sci.*, 2010, **35**(1), 107–113.
- 33 M. Crosera, A. Prodi, M. Mauro, M. Pelin, C. Florio and F. Bellomo, *et al.*, Titanium Dioxide Nanoparticle Penetration into the Skin and Effects on HaCaT Cells, *Int. J. Environ. Res. Public Health*, 2015, **12**(8), 9282–9297.
- 34 W. G. Kreyling, U. Holzwarth, C. Schleh, S. Hirn, A. Wenk and M. Schäffler, *et al.*, Quantitative biokinetics over a 28 day period of freshly generated, pristine, 20 nm titanium dioxide nanoparticle aerosols in healthy adult rats after a single two-hour inhalation exposure, *Part. Fibre Toxicol.*, 2019, **16**(1), 29.
- 35 M. D. Hoffman and A. Gelman, The No-U-Turn Sampler: Adaptively Setting Path Lengths in Hamiltonian Monte Carlo, *J. Mach. Learn. Res.*, 2014, **15**(47), 1593–1623.
- 36 Environmental Protection Agency (EPA), *Reference physiological parameters in pharmacokinetic modeling*, Office of Health and Environmental Assessment, Washington DC, 1988.
- 37 A. J. Koivisto, T. Hussein, R. Niemelä, T. Tuomi and K. Hämeri, Impact of particle emissions of new laser printers on modeled office room, *Atmos. Environ.*, 2010, **44**(17), 2140–2146.
- 38 C. Thiel, S. Schneckener, M. Krauss, A. Ghallab, U. Hofmann and T. Kanacher, *et al.*, A Systematic Evaluation of the Use of Physiologically Based Pharmacokinetic Modeling for Cross-Species Extrapolation, *J. Pharm. Sci.*, 2015, **104**(1), 191–206.
- 39 V. Gomez, M. Levin, A. T. Saber, S. Irusta, M. Dal Maso and R. Hanoi, *et al.*, Comparison of Dust Release from Epoxy and Paint Nanocomposites and Conventional Products during Sanding and Sawing, *Ann. Occup. Hyg.*, 2014, **58**(8), 983–994.
- 40 A. J. Koivisto, A. C. Ø. Jensen, K. I. Kling, J. Kling, H. C. Budtz and I. K. Koponen, *et al.*, Particle emission rates during electrostatic spray deposition of TiO₂ nanoparticle-based photoactive coating, *J. Hazard. Mater.*, 2018, **341**, 218–227.
- 41 A. J. Koivisto, K. I. Kling, A. S. Fonseca, A. B. Bluhme, M. Moreman and M. Yu, *et al.*, Dip coating of air purifier ceramic honeycombs with photocatalytic TiO₂ nanoparticles: A case study for occupational exposure, *Sci. Total Environ.*, 2018, **630**, 1283–1291.
- 42 D. A. Dankovic and E. D. Kuempel, *Occupational exposure to titanium dioxide*, National Institute for Occupational Safety and Health E and IDivision Titanium Dioxide Document Development Team, National Institute for Occupational Safety and Health E and IDivision, editors, 2011, Available from: <https://stacks.cdc.gov/view/cdc/5922>.
- 43 H. Shi, R. Magaye, V. Castranova and J. Zhao, Titanium dioxide nanoparticles: a review of current toxicological data, *Part. Fibre Toxicol.*, 2013, **10**(1), 15.
- 44 A. Afantitis, G. Melagraki, P. Isigonis, A. Tsoumanis, D. D. Varsou and E. Valsami-Jones, *et al.*, NanoSolveIT Project: Driving nanoinformatics research to develop innovative and integrated tools for in silico nanosafety assessment, *Comput. Struct. Biotechnol. J.*, 2020, **18**, 583–602.
- 45 O. T. Price, B. Asgharian, F. J. Miller, F. R. Cassee and R. de Winter-Sorkina, *Multiple Path Particle Dosimetry model (MPPD v1.0): A model for human and rat airway particle dosimetry, Mult Path Aerosol Dosim Model MPPD V10 Een Model Voor Dosim Van Aerosolen Luchtweegen Van Mens En Rat*, 2002.
- 46 H.-C. Yeh and G. M. Schum, Models of human lung airways and their application to inhaled particle deposition, *Bull. Math. Biol.*, 1980, **42**(3), 461–480.
- 47 C. J. E. Delmaar, W. J. G. M. Peijnenburg, A. G. Oomen, J. Chen, W. H. de Jong and A. J. A. M. Sips, *et al.*, A practical approach to determine dose metrics for nanomaterials, *Environ. Toxicol. Chem.*, 2015, **34**(5), 1015–1022.
- 48 H. M. Braakhuis, F. R. Cassee, P. H. B. Fokkens, L. J. J. de la Fonteyne, A. G. Oomen and P. Krystek, *et al.*, Identification of the appropriate dose metric for pulmonary inflammation of silver nanoparticles in an inhalation toxicity study, *Nanotoxicology*, 2016, **10**(1), 63–73.
- 49 EFSA Scientific Committee, A. Hardy, D. Benford, T. Halldorsson, M. J. Jeger and K. H. Knutsen, *et al.*, Update: use of the benchmark dose approach in risk assessment, *EFSA J.*, 2017, **15**(1), e04658.
- 50 L. T. Haber, M. L. Dourson, B. C. Allen, R. C. Hertzberg, A. Parker and M. J. Vincent, *et al.*, Benchmark dose (BMD) modeling: current practice, issues, and challenges, *Crit. Rev. Toxicol.*, 2018, **48**(5), 387–415.
- 51 European Food Safety Authority (EFSA), Guidance of the Scientific Committee on Use of the benchmark dose approach in risk assessment, *EFSA J.*, 2009, **7**(6), 1150.



- 52 D. A. Winkler, E. Mombelli, A. Pietroiusti, L. Tran, A. Worth and B. Fadeel, *et al.*, Applying quantitative structure–activity relationship approaches to nanotoxicology: Current status and future potential, *Nanotoxicology*, 2013, **313**(1), 15–23.
- 53 A. Gajewicz, K. Jagiello, M. T. D. Cronin, J. Leszczynski and T. Puzyn, Addressing a bottle neck for regulation of nanomaterials: quantitative read-across (Nano-QRA) algorithm for cases when only limited data is available, *Environ. Sci.: Nano*, 2017, **4**(2), 346–358.
- 54 K. Gerloff, B. Landesmann, A. Worth, S. Munn, T. Palosaari and M. Whelan, The Adverse Outcome Pathway approach in nanotoxicology, *Comput. Toxicol.*, 2017, **1**, 3–11.
- 55 A. J. Clippinger, A. Ahluwalia, D. Allen, J. C. Bonner, W. Casey and V. Castranova, *et al.*, Expert consensus on an in vitro approach to assess pulmonary fibrogenic potential of aerosolized nanomaterials, *Arch. Toxicol.*, 2016, **90**(7), 1769–1783.
- 56 P. Nymark, H. L. Karlsson, S. Halappanavar and U. Vogel, Adverse Outcome Pathway Development for Assessment of Lung Carcinogenicity by Nanoparticles, *Front. Toxicol.*, 2021, **3**, 21.

